

The relationship between galaxy and halo sizes in the Illustris and IllustrisTNG simulations

Tathagata Karmakar^{1,2,3}★ Shy Genel^{4,5}, Rachel S. Somerville⁴

¹Department of Physics and Astronomy, University of Rochester, Rochester, NY 14627, USA.

²Center for Coherence and Quantum Optics, University of Rochester, Rochester, NY 14627, USA.

³Institute for Quantum Studies, Chapman University, Orange, CA 92866, USA.

⁴Center for Computational Astrophysics, Flatiron Institute, 162 5th Ave, New York, NY 10010, USA

⁵Columbia Astrophysics Laboratory, Columbia University, 550 West 120th Street, New York, NY 10027, USA

26 January 2023

ABSTRACT

Abundance matching studies have shown that the average relationship between galaxy radius and dark matter halo virial radius remains nearly constant over many orders of magnitude in halo mass, and over cosmic time since about $z = 3$. In this work, we investigate the predicted relationship between galaxy radius r_e and halo virial radius R_h in the numerical hydrodynamical simulations Illustris and IllustrisTNG from $z \sim 0$ –3, and compare with the results from the abundance matching studies. We find that Illustris predicts much higher r_e/R_h values than the constraints obtained by abundance matching, at all redshifts, as well as a stronger dependence on halo mass. In contrast, IllustrisTNG shows very good agreement with the abundance matching constraints. In addition, at high redshift it predicts a strong dependence of r_e/R_h on halo mass on mass scales below those that are probed by existing observations. We present the predicted r_e/R_h relations from Illustris and IllustrisTNG for galaxies divided into star-forming and quiescent samples, and quantify the scatter in r_e/R_h for both simulations. Further, we investigate whether this scatter arises from the dispersion in halo spin parameter and find no significant correlation between r_e/R_h and halo spin. We investigate the paths in r_e/R_h traced by individual haloes over cosmic time, and find that most haloes oscillate around the median r_e/R_h relation over their formation history.

Key words: galaxies : formation – galaxies: evolution – galaxies: haloes

1 INTRODUCTION

In the modern paradigm for galaxy formation, galaxies form within dark matter haloes, overdense gravitationally bound dark-matter dominated structures within which gas accretes and cools (Somerville & Davé 2015). The *virial radius* of a dark matter halo is typically defined, somewhat arbitrarily, as the radius within which the mean overdensity with respect to the background (or critical) density of the Universe¹ is some factor Δ_{vir} . As the gas cools down sufficiently and condenses in the inner parts of halos, stars form and galaxies grow. Although the formation of dark matter haloes is fairly well understood and quantified through numerical simulation, our understanding of the baryonic processes that shape galaxy properties, such as star formation, stellar feedback, mergers, black hole growth and Active Galactic Nucleus (AGN) feedback, remains very incomplete (Somerville & Davé 2015; Naab & Ostriker 2017). While the physics of galaxy formation seems exceedingly complex, the Universe provides us with clues to its underlying simplicity in the form of *scaling relations*. These are tight observed relationships between galaxy global properties, such as stellar mass and metallicity,

or global and structural properties, such as stellar mass and galaxy radius. The latter is the underlying focus of this study.

Abundance matching is a well established empirical technique for constraining the relationship between galaxy and dark matter halo properties, within the paradigm in which galaxies are always hosted by DM haloes or sub-haloes (for a recent review see Wechsler & Tinker 2018). Sub-haloes are haloes that have merged into and are orbiting within a larger virialized halo. In traditional Sub-halo Abundance Matching (SHAM), one derives a mapping between galaxy stellar mass (or luminosity) and dark matter halo mass (m_*/M_h), using the (sub)halo mass function predicted by N-body simulations and an observed stellar mass (luminosity) function (e.g. Moster et al. 2010; Behroozi et al. 2010; Rodriguez-Puebla et al. 2017). In *structural* SHAM, one takes this a step further by deriving a mapping between DM halo radius and galaxy radius, by adopting a SMHM relation (with some dispersion) and requiring that the model matches the observed size-mass relation. In this way, Kravtsov (2013) showed that the relationship between galaxy size and halo virial radius (r_e/R_h) is consistent with a nearly constant average value across many orders of magnitude in mass and for galaxies of diverse morphology, from giant ellipticals to low mass dwarfs. Several later studies expanded this approach to high redshift (Shibuya et al. 2015; Huang et al. 2017; Somerville et al. 2018). In particular, Somerville et al. (2018, hereafter S18) carefully combined observations from $z \sim 0$ with high

★ tkarmaka@UR.Rochester.edu

¹ Conventions regarding halo definitions vary; see Section 2 for details.

redshift observations in a consistent manner, and also quantified the conditional size *distributions*, as well as the mean r_e/R_h relation. S18 showed that the nearly linear relation between r_e and R_h holds up to $z \sim 3$, with only weak evolution in the value of the ratio r_e/R_h . We focus on the S18 abundance matching results in this work, but they are broadly consistent with those of other studies in the literature.

The results of the structural abundance matching studies mentioned above were unexpected, and prompted many open questions, including the following. 1) Why should the ratio between galaxy size and halo size be close to constant over many orders of magnitude in halo mass and many billions of years in cosmic time? This is especially mysterious given that the halo virial radius is in many ways an arbitrary quantity. 2) What can we learn from the empirical constraints on r_e/R_h about the physical processes that shape the structural properties of galaxies? 3) What is the origin of the *dispersion* in r_e/R_h at fixed halo mass²? Can this be connected to a second or higher order halo parameter beyond mass? 4) What kind of paths in r_e/R_h space do galaxies trace over cosmic time? Does a given object tend to always be high or low relative to the average r_e/R_h over its whole history, or do galaxies oscillate around the mean r_e/R_h relation?

In the classical picture of disc formation, dark matter haloes acquire angular momentum via quadrupole interactions with neighboring proto-galaxies (Peebles 1969). One can define a dimensionless spin parameter for a halo with angular momentum J , energy E and mass M (see Peebles 1969):

$$\lambda = \frac{J|E|^{1/2}}{GM^{5/2}} \quad (1)$$

which describes how rotationally supported the halo is. Analytic models employing the angular momentum partition ansatz assume that hot gas is “spun up” during the halo formation, and therefore has the same specific angular momentum as the DM halo, and that the specific angular momentum of the gas is conserved as it collapses to form a disc. Under the simplest set of assumptions, one expects the size of a disc forming under these conditions to obey a proportionality with the product of the halo spin and the halo radius: $r_e \propto \lambda R_h$ (Mo et al. 1998; Dalcanton et al. 1997; Somerville et al. 2008). Numerous refinements to the simplest models have been developed in the literature, accounting for complications such as deviation of the halo gas profile from an isothermal sphere, modification of the inner halo profiles by gravity or energy input from stellar feedback, and transfer of angular momentum during the disc formation process (Blumenthal et al. 1986; Flores et al. 1993; Dutton et al. 2007). For a more detailed summary of these models, see S18 Section 5.4; however, we note that all of these models predict a fairly strong linear relationship between r_e and λR_h , modulated by other parameters such as the halo concentration and the disc baryon fraction. Moreover, S18 showed that the conditional size relation (the distribution of galaxy sizes in a given stellar mass bin) is remarkably similar to the distribution of λR_h in their SHAM, providing an indirect suggestion that the dispersion in galaxy size at fixed stellar mass is consistent with being due to a proportionality between r_e and λR_h .

Modern numerical hydrodynamic simulations set within a cosmological context are a powerful tool to gain more insights into the physical processes behind the observed scaling relations. These simulations have demonstrated that galaxy internal structures, including

size, are very sensitive to the details of the baryonic processes implemented in the simulations, in particular stellar and black hole feedback. Reproducing the observed size-mass relation for galaxies was a challenge for the earliest generations of numerical hydrodynamic simulations, which tended to produce galaxies that were too compact and bulge dominated (Sommer-Larsen et al. 1999; Navarro & Steinmetz 2000; Steinmetz & Navarro 2002). The more recent generation of cosmological hydrodynamic simulations have demonstrated quite good success at reproducing the observed size-mass relation and its evolution over cosmic time (Brooks et al. 2011; Furlong et al. 2017; Genel et al. 2018).

All current cosmological hydrodynamic simulations contain phenomenological “sub-grid” recipes to model processes that cannot be simulated explicitly, such as the formation of stars out of dense gas, the driving of galaxy-scale winds by massive stars and supernovae explosions, and accretion onto supermassive black holes (Somerville & Davé 2015). These sub-grid recipes contain adjustable parameters that are tuned to match a set of observations. Global properties, such as the galaxy stellar mass function, are often used for this purpose. It is particularly intriguing that a set of parameters that reproduces such global properties may not reproduce structural properties: for example, in the original Illustris simulations (Vogelsberger et al. 2013), which were tuned to match a set of global properties, the predicted galaxy sizes were about a factor of two larger than observations indicate (Genel et al. 2014). In the updated IllustrisTNG simulations, the relationship between stellar mass and halo mass remains very similar to that in the original Illustris simulations, but the predicted sizes are significantly smaller (Pillepich et al. 2018a; Genel et al. 2018). Although it is now well established that galaxy sizes are sensitive to both stellar and AGN feedback, many of the details of how physical processes like feedback shape galaxy sizes remain unclear.

In this paper, we use the Illustris and IllustrisTNG simulations as laboratories to study the relationship between galaxies and their host dark matter haloes. Although many works have studied the predictions of numerical simulations for the observed galaxy size-mass relation, as noted above, there has been little work quantifying the relationships between DM halo properties and galaxy properties, such as the stellar mass vs. halo mass relation and galaxy size vs. halo size relation, in physics-based simulations. We compare the stellar mass vs. halo mass and galaxy size vs. halo size relations extracted from Illustris and IllustrisTNG with the abundance matching results of S18 over a range of cosmic time ($z \sim 3-0$). We quantify the galaxy-size vs. halo size relation for star-forming and quiescent galaxies in the simulations. Abundance matching techniques have a limited ability to constrain the *dispersion* in these relationships, which can be measured directly in the simulations. This result provides an important input for empirical models. In addition, we attempt to understand the *physical origin* of the dispersion in these relations, by examining whether the dispersion in size at fixed mass is correlated with halo spin in the simulations. We further explore the origin of the dispersion by tracing the growth of individual galaxies over cosmic time.

In section 2, we present a brief summary of the abundance matching method and results of S18. In section 3 we provide a brief background on the Illustris and IllustrisTNG simulations. We present our main results in section 4. We discuss the interpretation of our results, and their relationship with previous results in the literature in section 5, and summarize our key findings and conclude in section 6.

² Recall that for any given overdensity-based definition of the virial radius, virial mass and radius are perfectly interchangeable as there is zero scatter in the relationship between them.

2 SUB-HALO ABUNDANCE MATCHING METHOD AND RESULTS

In the simplest version of (sub)-halo abundance matching, one takes a population of dark matter haloes from a dissipationless N-body simulation and orders them by mass. One then takes a population of galaxies from an observational sample, orders them by the global property (such as stellar mass or luminosity), and assumes that the most massive (luminous) galaxy occupies the most massive halo, the second most massive galaxy occupies the second most massive halo, etc. This procedure, however, does not account for possible dispersion in the stellar mass vs. halo mass (SMHM) relation. More recent works instead fit for the parameters in a function describing the mean SMHM relation ($\langle m_*(M_h) \rangle$) in order to minimize the deviation between the model stellar mass function and an observed stellar mass function (Rodríguez-Puebla et al. 2017; Moster et al. 2018; Behroozi et al. 2019). The dispersion in m_* as a function of M_h and redshift z is also parameterized, and these parameters are constrained in the modeling procedure. Most SHAM studies also fit for galaxy clustering properties, which provide some constraints on the dispersion in $m_*(M_h)$. S18 adopt the SMHM relation and stellar mass dispersion relations from Rodríguez-Puebla et al. (2017). Note that both S18 and Rodríguez-Puebla et al. (2017) adopt the definition of halo mass and virial radius $M_{\text{vir}} = \frac{4}{3} \Delta_{\text{vir}} \rho_{\text{crit}} R_{\text{vir}}^3$, where Δ_{vir} is given by Eqn. 6 of Bryan & Norman (1998) and ρ_{crit} is the critical density of the Universe.

S18 then used a “forward modeling” approach to constrain the median relationship between galaxy size and halo size as follows. They created a mock catalog based on the Bolshoi-Planck dissipationless N-body simulation (Rodríguez-Puebla et al. 2016) by assigning a stellar mass to each halo and sub-halo, including scatter as described above. They then binned their sample in stellar mass, and found the median halo radius in each bin. They then computed the median observed galaxy size in the same stellar mass bin. In this way, they obtained the median relation r_e/R_h . Other studies, such as Kravtsov (2013) and Huang et al. (2017), have carried out a similar analysis using somewhat different techniques (see S18 for an extensive discussion of the differences), and obtained qualitatively similar results for r_e/R_h . In “backwards modeling”, halo properties corresponding to an observational sample of galaxies are obtained by inverting a SHMR relation. As the SHMR becomes shallower at high halo masses, a positive deviation in stellar mass causes a larger deviation in halo mass than a comparable negative deviation does. Thus, in the presence of scatter in the SHMR, “backwards modeling” leads to an overestimate in halo mass and sizes, making “forward modeling” a more reliable strategy (see S18 for a detailed discussion).

The observational samples used to obtain the size-mass relations adopted in S18 come from DR2 of the Galaxy And Mass Assembly Survey (GAMA; Liske et al. 2015), which is an optically selected survey of nearby galaxies ($0.01 < z < 0.12$), and the CANDELS survey (Grogin et al. 2011; Koekemoer et al. 2011), which is based on observations with the WFC3 camera on the Hubble Space Telescope and probes galaxies out to high redshift ($z \sim 3$ in the study of S18). In both cases, stellar masses are estimated from the photometry using standard techniques. Also in both cases, the observed projected semi-major axis half-light radii in a fixed rest-frame band ($r_{e,\text{obs}}$) from the studies of Lange et al. (2015) and van der Wel et al. (2014a) are converted to 3D half stellar mass radii ($r_{*,3D}$) using the formula $r_{e,\text{obs}} = f_p f_k r_{*,3D}$. Here f_p accounts for the projection from 3D to 2D, and f_k accounts for between conversion half-light radii and half stellar mass radii. In S18, a value of $(f_p f_k)_{\text{disk}} = 1.2$ has been adopted for disk galaxies (i.e. galaxies with Sérsic index $n_s <$

2.5), while a value of $(f_p f_k)_{\text{spheroid}} = 0.78$ has been adopted for spheroids ($n_s > 2.5$). Since f_p depends on galaxy shapes, it has the potential to introduce additional stellar mass and redshift dependence in $r_{e,\text{obs}}/r_{*,3D}$. The values of f_k are found to lie between 1.12 – 1.5 and do not show any significant dependence on galaxy mass or redshift (see Lange et al. (2015) and Wuyts et al. (2012)). See S18 for a more detailed discussion of the projected light to 3D stellar mass size conversion procedure and references for the adopted parameter values.

S18 and Kravtsov (2013) found the striking result that the average relationship between galaxy size and halo virial radius r_e/R_h at $z = 0$ remains nearly constant over several orders of magnitude in halo mass. This result is particularly surprising given that the galaxy population is dominated by disc-like galaxies at lower stellar (halo) masses (see Figure 4 in S18), but dominated by elliptical type galaxies at higher masses, and these objects are thought to form in very different ways. S18 and Huang et al. (2017) further showed that this average ratio r_e/R_h remains nearly independent of halo mass out to high redshift $z \sim 3$, and its value evolves only mildly with redshift over this period of more than 10 billion years in cosmic time.

These studies have left some open questions. First, some studies (Kravtsov (2013) and Huang et al. (2017)) present results for r_e/R_h for galaxies dis-aggregated into disc-dominated and spheroid dominated types. However, this relies on the assumption that the SMHM relation for these different types of galaxies is the same, which may not be the case (Cui et al. 2021). Second, none of these studies are able to constrain the dispersion in r_e/R_h . Third, the physical reason that all types of galaxies over such a large range in halo mass and redshift should obey this nearly universal relationship between the size of their stellar body and the virial radius of their dark matter halo remains unclear.

3 THE SIMULATED GALAXY POPULATIONS

Illustris (Genel et al. 2014; Vogelsberger et al. 2014a,b) and IllustrisTNG (Marinacci et al. 2018; Naiman et al. 2018; Nelson et al. 2018; Pillepich et al. 2018b; Springel et al. 2018) are suites of hydrodynamical simulations of galaxy formation and evolution in large cosmological volumes. Here we focus on the highest-resolution levels of the ($\sim 100 \text{ Mpc}$)³ volume from each of these suites, which we hereafter refer to simply as Illustris and IllustrisTNG. Both employ the quasi-Lagrangian code AREPO to evolve up to a total of $\sim 2 \times 1820^3$ resolution elements representing both dark matter and baryons in a ($75h^{-1} \text{ Mpc}$)³ volume. Dark matter is assumed to be collisionless and the N-body problem is solved using a TreePM method. For the hydrodynamical evolution, the volume is discretized using a Voronoi tessellation whose mesh-generating points move and (de)refine in a quasi-Lagrangian manner. Further, the simulation takes into account various physical processes that are believed to be critical for galaxy formation. These processes include radiative cooling, star formation after gas crosses a critical number density threshold of 0.13 cm^{-3} , metal enrichment through stellar evolution, feedback of gas into the circumgalactic medium via galactic winds, and the feedback associated with supermassive black holes (SMBH) at the centers of galaxies (see Vogelsberger et al. 2013; Weinberger et al. 2017; Pillepich et al. 2018a).

Despite showing good qualitative agreement with many observational results, some predictions from Illustris are in tension with observations, such as larger galaxy sizes compared to the observations, and overprediction of the number density of both high and low mass galaxies at $z \sim 0$. IllustrisTNG attempts to address some of

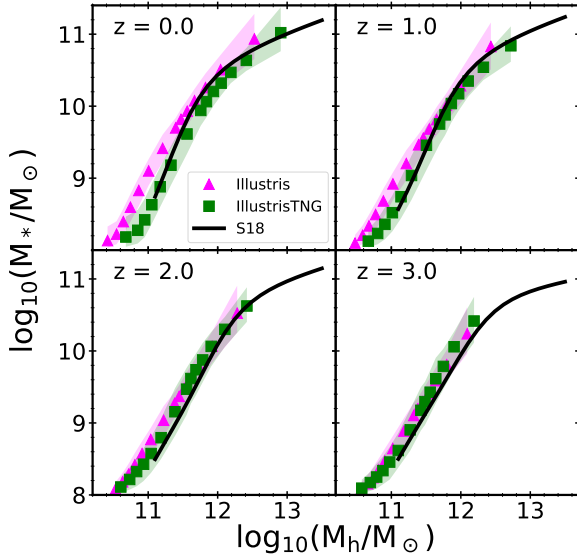


Figure 1. Comparison of stellar-to-halo mass relations predicted by the Illustris and IllustrisTNG simulations (pink triangles and green squares, respectively) and that adopted in the SHAM of S18 (black lines), in several redshift bins from $z = 0$ to 3 as indicated on the panels. The symbols show the medians from the simulations, and shaded areas show the 16th and 84th percentiles. The stellar to halo mass relations are very similar in the two simulations, and agree well with the SHAM results.

these issues by adopting a few key differences in some of the physical processes. These include modeling of magnetic fields (via the ideal MHD approximation), adding more flexibility to the galactic wind model, replacing the thermal bubble model for AGN feedback at low accretion rates with a kinetic AGN feedback model, increasing the black hole seed mass and removing the black hole accretion artificial boost factor. The cosmological parameters have also been slightly updated in IllustrisTNG ($\Omega_m = 0.3089$, $\Omega_\Lambda = 0.6911$, $\Omega_b = 0.0486$, $\sigma_8 = 0.8159$ and $h = 0.6774$) compared to Illustris ($\Omega_m = 0.2726$, $\Omega_\Lambda = 0.7274$, $\Omega_b = 0.0456$, $\sigma_8 = 0.809$ and $h = 0.704$).

The objects we refer to as galaxies in this work are identified using the SUBFIND algorithm (Springel et al. 2001), which finds self-bound objects around peaks in the density field. When referring to virial properties of the host haloes, we employ a definition corresponding to a spherical region around the most bound particle in the halo that contains a total matter overdensity of Δ_{vir} (as given by Eqn. 6 of Bryan & Norman (1998)) with respect to the critical density of the universe. Galaxy 3D sizes r_e are defined as the radius of a sphere that contains half of the total stellar mass, while the standard stellar mass value we use for each galaxy is the mass of stars within twice its r_e . Since we focus on relations between galaxies and their host haloes, we only study central galaxies, and we focus on those with stellar masses larger than $10^8 M_\odot$, which are well-resolved in the ($\sim 100 \text{ Mpc}$)³ volumes we employ.

4 RESULTS

4.1 Comparison with Abundance Matching Results

We start by comparing the median relationships between stellar mass and halo mass with the abundance matching results of S18 for both

the Illustris and IllustrisTNG simulations. Figure 1 shows the stellar-halo mass relation (SHMR) of the two simulations compared with that adopted in S18. We note the very good agreement between, in particular, the IllustrisTNG predictions and the SHAM results at all redshifts. Although IllustrisTNG was tuned, in part, to match the stellar mass function at $z = 0$, it was not explicitly tuned to match stellar mass functions at high redshift. At low redshift and low halo masses, the galaxy masses in Illustris are slightly higher at fixed halo mass than those in IllustrisTNG. This reflects the higher abundances of low mass galaxies predicted by the original Illustris simulation relative to observational constraints, which the revised physics in TNG was designed to mitigate. At $z > 1$, the SHMR relations predicted by the two simulations are nearly indistinguishable.

Next we investigate the relationship between r_e/R_h and stellar mass or halo mass. Figure 2 shows r_e/R_h vs. stellar mass on the left panel and r_e/R_h vs. halo mass on the right panel. The IllustrisTNG simulation is consistent with the relatively constant behavior of r_e/R_h with stellar and halo mass given by SHAM over the mass range where there are observational constraints. Interestingly, however, at lower masses and especially at high redshift, the simulations predict a significant increase in r_e/R_h with decreasing mass. The original Illustris simulation not only predicts a higher normalization for r_e/R_h than IllustrisTNG — consistent with the well-known tendency of original Illustris to produce galaxies with sizes that are too large compared with observations — but it also predicts a stronger dependence of r_e/R_h on halo mass than IllustrisTNG. This is very interesting, as it suggests that the very flat behavior of r_e/R_h with halo mass implied by the SHAM (and perhaps pertaining in the real Universe) may not be very generic.

Figure 3 shows r_e/R_h as a function of redshift for two different stellar mass bins ($10^{9.5} - 10^{10} M_\odot$ on the left, $10^{10.5} - 10^{11} M_\odot$ on the right) for both the Illustris and IllustrisTNG simulations, and the SHAM. The IllustrisTNG simulation shows qualitatively very similar behavior to the SHAM results, indicating a mild increase in r_e/R_h with cosmic time for the lower mass bin, and a mild decrease for the higher mass bin. Once again, the normalization of r_e/R_h is much higher at all redshifts for Illustris than for IllustrisTNG or the SHAM (in particular at lower masses), but the redshift dependence is similar. The dispersion in r_e/R_h is also somewhat higher in the original Illustris simulation.

As discussed in the Introduction, it is interesting to ask whether these relations, both between stellar mass and halo mass, and that between galaxy size and halo size, differ for galaxies of different types. Here, we use star formation activity to divide galaxies into star-forming and quiescent categories, as it has been found that these two categories have distinct stellar size-mass relations (van der Wel et al. 2014b). To define star-forming galaxies, we follow a procedure similar to the one introduced by Brennan et al. (2015). Namely, we examine the median specific star formation rates (ssfr) of galaxies with stellar masses $10^9 - 10^{9.5} M_\odot$ and $10^{9.5} - 10^{10} M_\odot$, at a given redshift. Then, as a function of stellar mass, we define a line by assigning these two ssfr values to stellar masses $10^{9.25} M_\odot$ and $10^{9.75} M_\odot$ respectively. Galaxies with specific star formation rates higher than 25% of the values denoted by the line are considered star-forming for our analysis, while the rest are considered quiescent galaxies. Such a definition results in a threshold between quenched and starforming galaxies of $10^{-10.40} \text{ yr}^{-1}$ at $10^{9.25} M_\odot$ and $10^{-10.45} \text{ yr}^{-1}$ at $10^{9.75} M_\odot$, which captures the slope of the main sequence in the simulations, and is similar to values typically used in the literature to define the quenching threshold. First, we examine the relation between stellar mass and halo mass for the two types of galaxies in Figure 4, which shows Illustris on the left and IllustrisTNG on the right panel. We

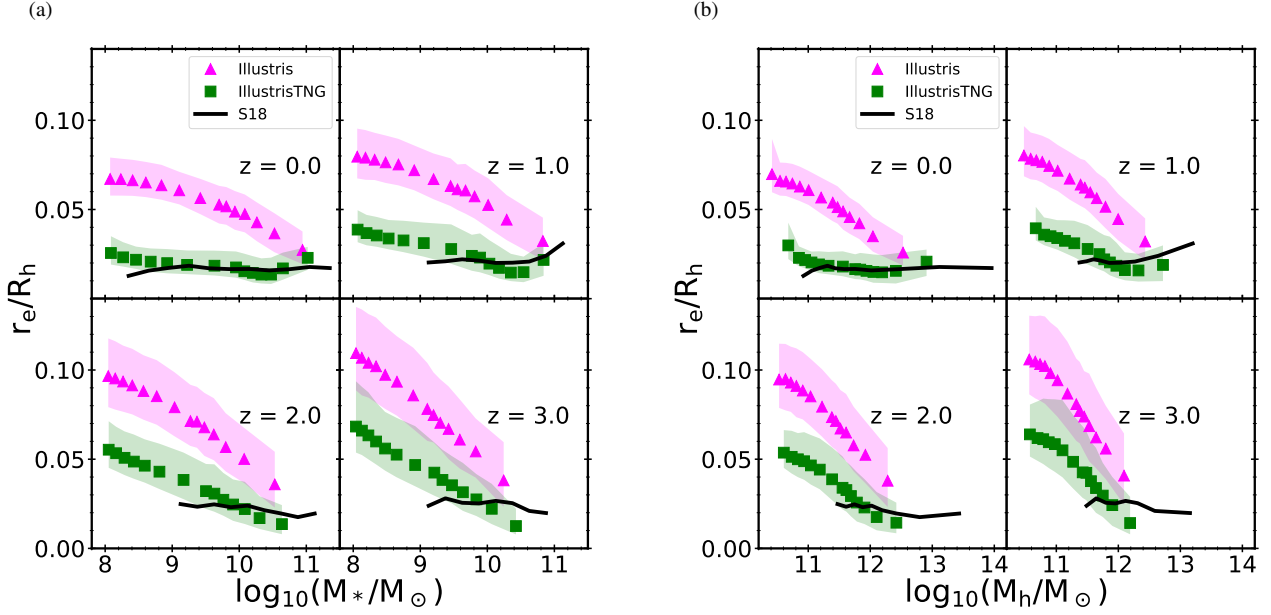


Figure 2. Galaxy radius to halo radius ratio r_e/R_h of central galaxies versus stellar (left) and halo mass (right). Magenta (green) symbols represent the medians from the Illustris (IllustrisTNG) simulation and corresponding shaded regions represent 16th and 84th percentiles. Black curves show the SHAM results from S18. At low redshifts, the IllustrisTNG r_e/R_h relation is rather flat, and agrees well with the SHAM results. However, at high redshifts both simulations show a stronger dependence of r_e/R_h on mass, in mild tension with the flat SHAM results.

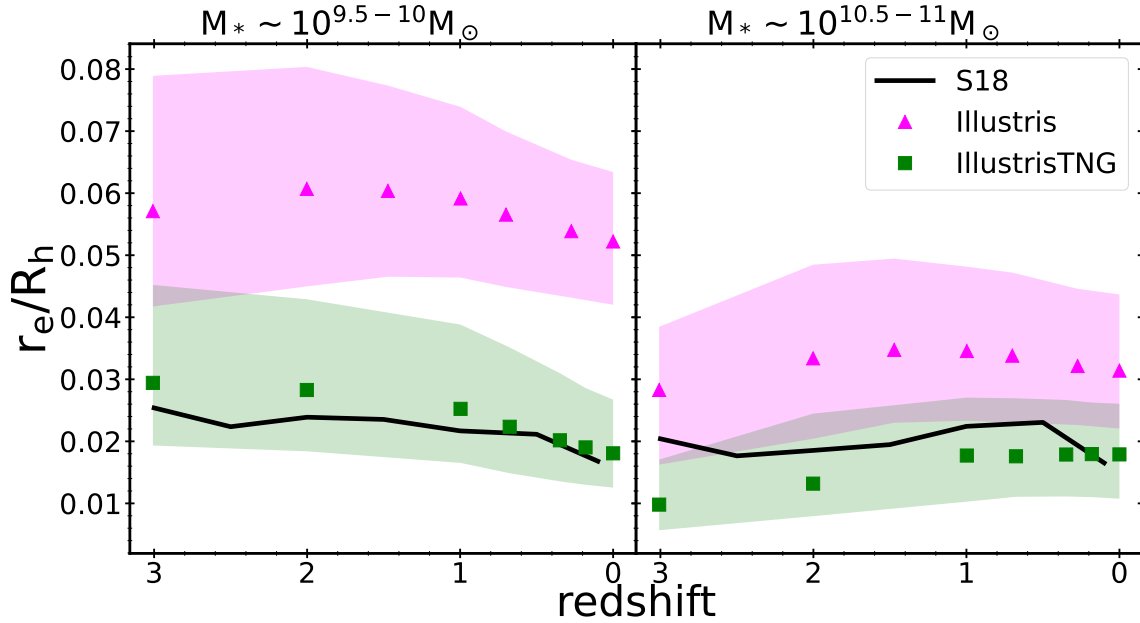


Figure 3. Galaxy radius to halo radius ratio as a function of redshift for Illustris, IllustrisTNG and the S18 SHAM for stellar mass bins $10^{9.5-10} M_\odot$ (left) and $10^{10.5-11} M_\odot$ (right). All three models show weak, qualitatively similar redshift evolution.

can see that the median SMHM relations are nearly indistinguishable for star-forming and quiescent galaxies in both simulations, although the dispersion is higher for quiescent galaxies. Next, in Figure 5, we show r_e/R_h for star-forming and quiescent galaxies separately as a function of both stellar mass and halo mass. In the original Illustris simulation, r_e/R_h is very similar for star-forming and quiescent

galaxies, except that quiescent galaxies have an upturn in r_e/R_h at very low halo masses (note there are no quiescent galaxies in the highest redshift bin of Illustris, $z = 3$). For IllustrisTNG, r_e/R_h for star-forming and quiescent galaxies are almost indistinguishable, with only a hint of a slight deviation in the lowest halo mass bin for quiescent galaxies at $z = 1$ and $z = 0$.

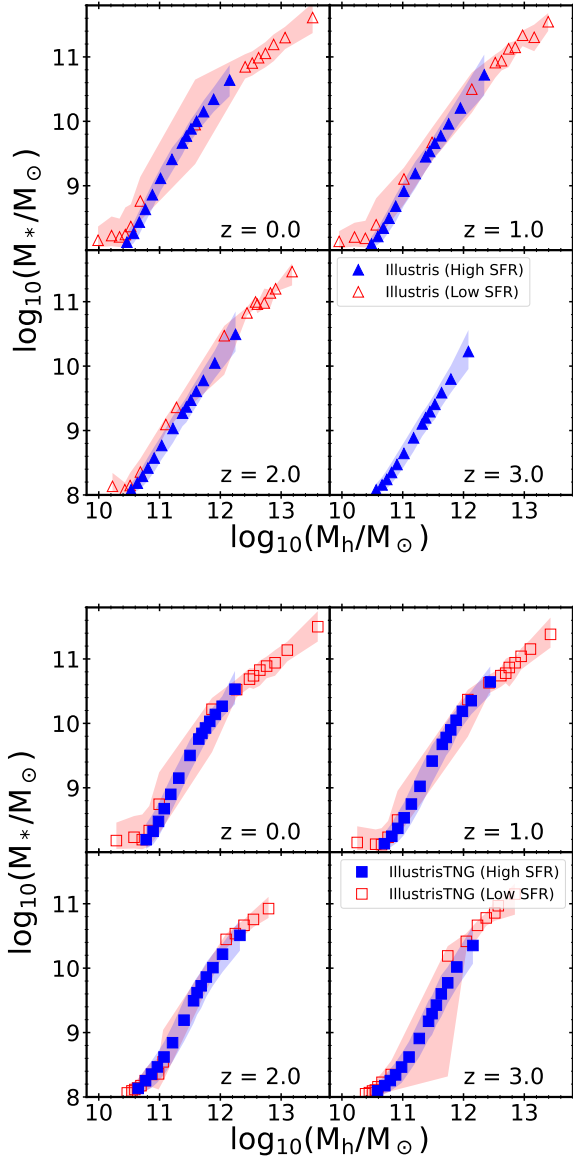


Figure 4. Stellar-to-halo mass relation for Illustris (top) and IllustrisTNG (bottom). The red symbols represent low-SFR galaxies and the blue represent high-SFR ones. Corresponding shaded regions represent 16th to 84th percentiles. At $z = 3$, for Illustris, low-SFR galaxies are not shown due to their extreme scarcity. In both simulations, the SMHM relation is very similar for high- and low-SFR galaxies.

4.2 Investigation of the dispersion

We now turn our attention to the dispersion in r_e/R_h seen in both simulations in Figure 2. The two panels in Figure 6 show the scatter in r_e/R_h as a function of stellar mass on the left and halo mass on the right for the Illustris and IllustrisTNG simulations. The dispersion is calculated by taking the difference between the 84 and 16 percentile values and then dividing by 2. Illustris consistently shows higher dispersions than IllustrisTNG at all redshifts. At low redshifts ($z \sim 0 - 1$), the dispersion is nearly constant across all stellar and halo

masses. However, the dispersion shows a decreasing trend for high mass galaxies at high redshifts.

This raises the question: what is the physical origin of this dispersion in galaxy size at fixed stellar or halo mass? Is the dispersion the result of dependence on a second or higher order parameter of the halo? Or is it a result of different evolutionary paths experienced by different galaxies? As noted in the Introduction, in the classical picture of disc formation, the DM halo spin is expected to be an important second parameter in determining the galaxy size. To explore this correlation in IllustrisTNG, we define the residual $\Delta \log_{10}(r_e/R_h)$ as the difference between the log size ratio and the median log size ratio for a given stellar mass bin and redshift. We then plot this residual against the halo spin parameter, defined as in Eqn. 2 and calculated from the IllustrisTNG simulation itself (rather than its DM-only analog). We show this relationship in Figure 7, and display the Spearman rank correlation coefficient in each panel. It is apparent that $\Delta \log_{10}(r_e/R_h)$ does not show a strong correlation with the spin parameter. For low mass galaxies, the correlation coefficient increases with redshift. For high mass galaxies, there does not seem to be a clear trend with redshift.

The preceding analysis shows $\Delta \log_{10}(r_e/R_h)$ at a snapshot in time for different redshifts. However, it is interesting to know whether an individual galaxy with high (or low) $\Delta \log_{10}(r_e/R_h)$ has always been high (or low) over its entire history, or do galaxies tend to frequently cross the line of zero residual, i.e., oscillate around the mean relation? In order to investigate this, we utilize merger trees that trace the main progenitor of each galaxy or halo back in time (Rodríguez-Gomez et al. 2015). We select galaxies from IllustrisTNG according to their $z = 0$ stellar mass, and show the tracks in $\Delta \log_{10}(r_e/R_h)$ with redshift for a selection of objects in several stellar mass bins in Figure 8. The residuals are calculated as the difference between the value of r_e/R_h for a particular object and the median value for the same stellar mass at the same redshift. Also, for specific mass bins, the values of the dispersion (half of the distance between the 16th and 84th percentiles) as functions of redshifts (as shown in Figure 6) are also shown above and below the zero residual line. As we move towards higher redshifts following the tracks, the masses of the sample galaxies tend to deviate from the specified mass bins, therefore causing a divergence in the trajectories. From this Figure, we get the impression that most galaxies tend to cross the median (i.e. $\Delta \log_{10}(r_e/R_h) = 0$) at least once over their lifetime.

To quantify this more robustly, we record the number of times that each galaxy crosses the r_e/R_h median line during its lifetime between $z = 3$ to $z = 0$, for four different stellar mass bins in IllustrisTNG, and show the distributions of these crossing counts as histograms in Figure 9. This confirms that most galaxies ($\sim 60\%-75\%$) cross the median line at least once. We also notice that the distribution becomes more skewed towards small values for higher mass bins, suggesting that massive galaxies tend not to cross the median as many times during their evolution.

Equipped with the insights on how many times galaxies tend to oscillate around the median, we now look at how galaxies are positioned with respect to the median on average during their evolution. Figure 10 shows the histogram of time averaged residuals of r_e/R_h for different stellar mass bins. The residuals are calculated as before, then averaged over all the snapshots. We see that in all cases, the distributions lie within the average dispersion for different redshifts. Also, the distributions are peaked around the average residual of zero. If most of the galaxies were on the same side of the median radii ratio throughout their history, we would expect to see distributions with widths comparable to the average dispersions displayed. Thus, we infer that most of the galaxies tend to oscillate around the median

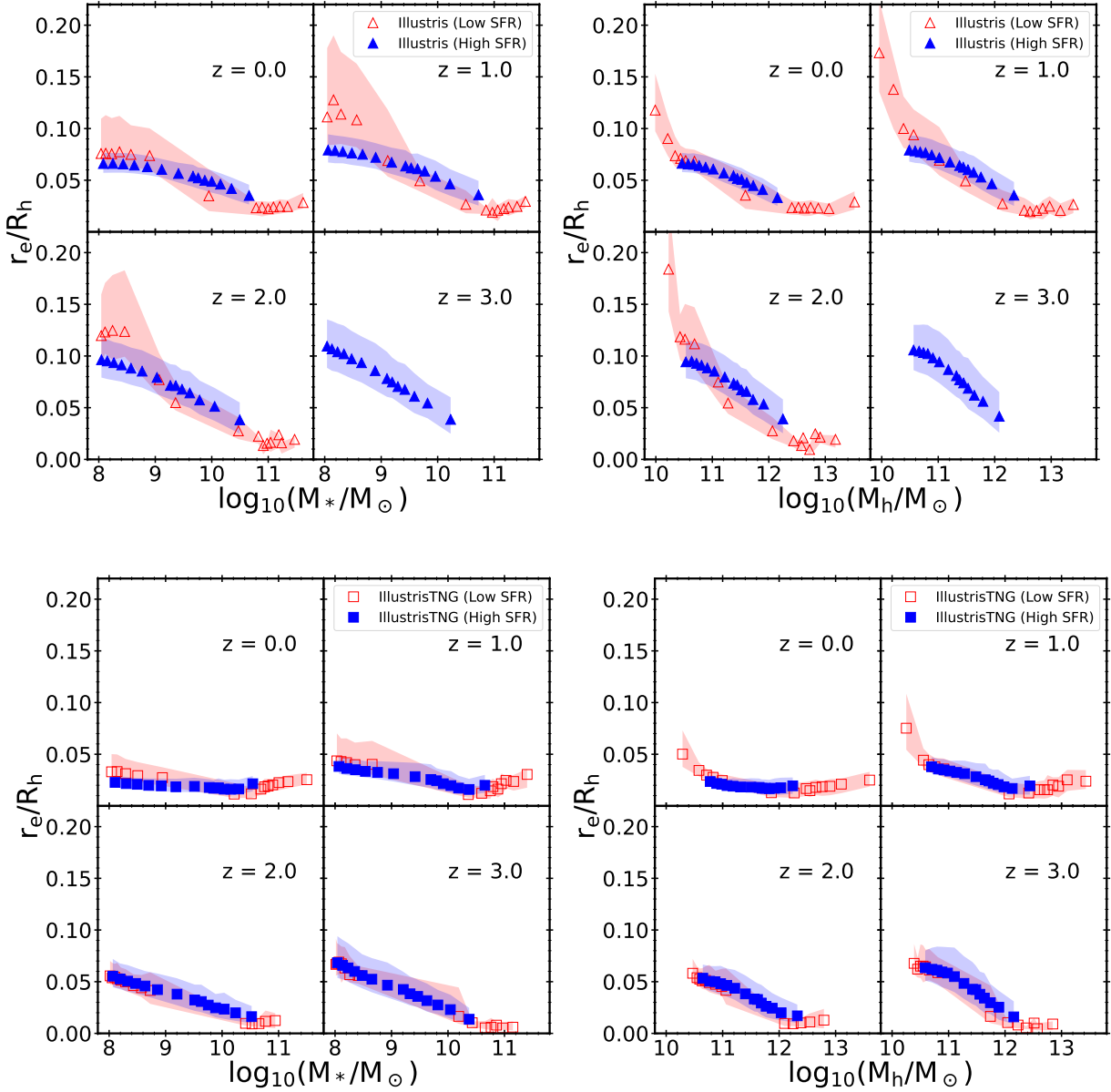


Figure 5. The stellar-to-halo size ratio r_e/R_h of central galaxies versus stellar mass (left) and halo mass (right). The top half presents results from the Illustris simulation, and the bottom from IllustrisTNG. The red (blue) symbols represent the medians for galaxies with low (high) SFRs, and the corresponding shaded regions represent the 16-84 percentile spread. Illustris shows a small difference between r_e/R_h for low and high-SFR galaxies at the lowest masses, but there is no discernible difference between the two for IllustrisTNG.

several times during their evolution. Our conclusion is also supported by the findings in Figure 9. We also see that the distributions become more and more skewed towards low values as we go to higher stellar masses, suggesting high mass galaxies with smaller sizes are more clustered near the median compared to the larger ones. It is worth noting that the vertical dispersion lines in Figure 10 are calculated from all the galaxies of a particular mass and redshift from the IllustrisTNG simulations. Whereas, the histograms include only galaxies that are on the main progenitor branch of a $z = 0$ galaxy. However, we have verified that this subtle distinction between the two samples does not cause any significant difference in the results.

5 DISCUSSION

5.1 Comparison with abundance matching results

We have analyzed a matched set of numerical cosmological simulations, Illustris and IllustrisTNG, in which many of the physical processes are in common, but some have been altered. This provides an interesting laboratory to study the relationship between galaxy and halo properties, and how these relationships differ in two simulations with the same underlying gravity and hydrodynamic solvers, but different implementations of physical processes. We compared the simulation predictions for the stellar to halo mass ratio m_*/M_h

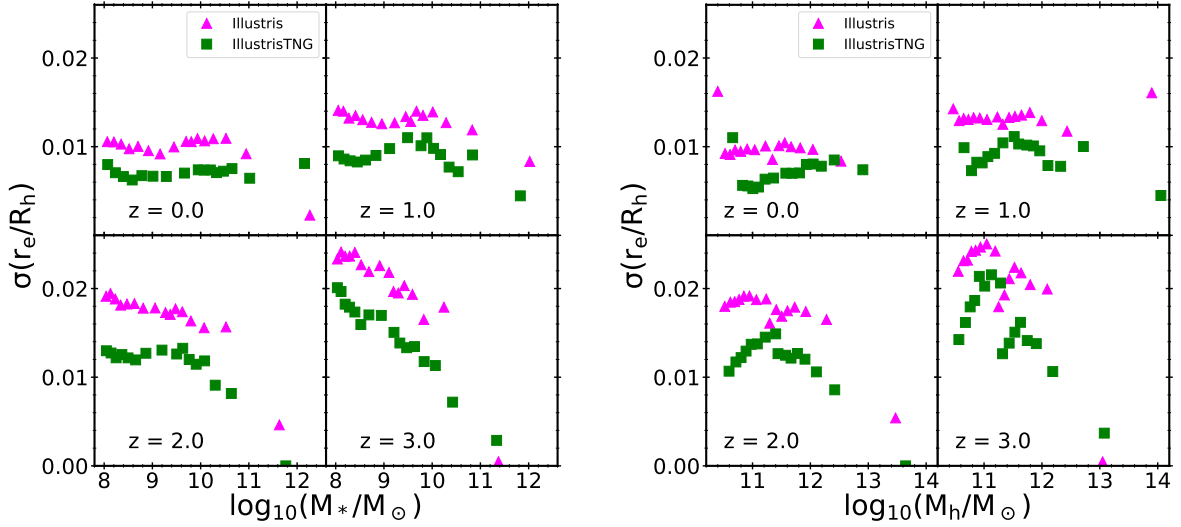


Figure 6. The dispersion of the stellar-to-halo size ratio as a function of stellar (halo) mass on the left (right). Here the dispersion is defined as half of the 84 to 16 percentile spread. Magenta (green) symbols show the results from Illustris (IllustrisTNG). IllustrisTNG shows somewhat smaller dispersions in r_e/R_h overall relative to Illustris.

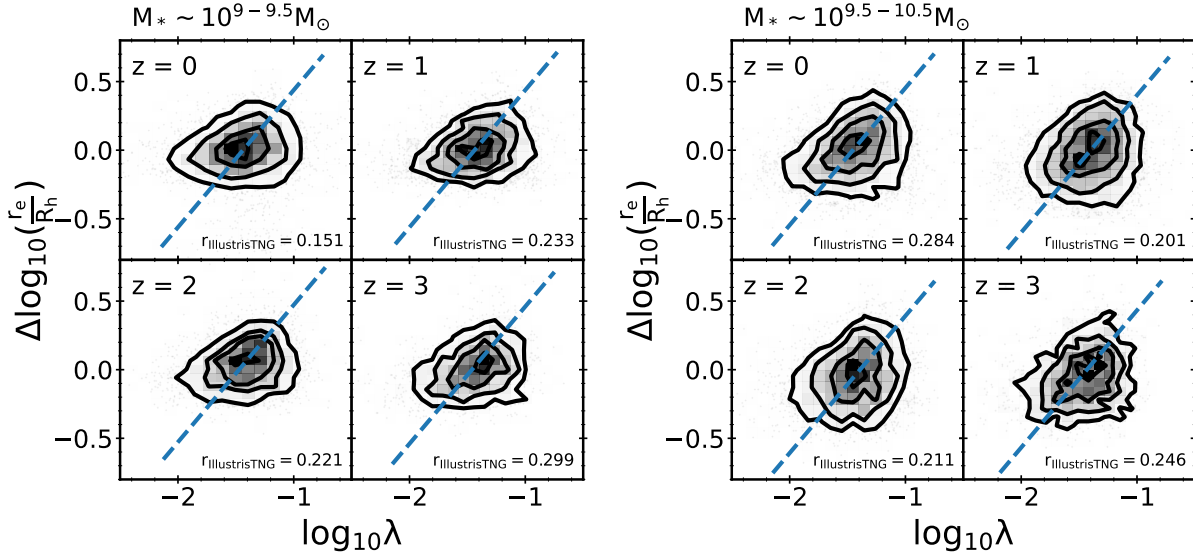


Figure 7. Residuals of the log stellar-to-halo size ratio r_e/R_h in IllustrisTNG versus log halo spin parameter for two different stellar mass bins and four different redshifts, as indicated on the panels. The blue dashed line specifies the unit slope linear relation between these quantities. Spearman's rank correlation coefficients are indicated on the individual panels, showing that the correlation between galaxy size and halo spin parameter in IllustrisTNG is weak.

and the galaxy size to halo size ratio r_e/R_h , and also compared these predictions with constraints from the structural abundance matching study of S18. We further compared both relations for galaxies divided into star-forming and quiescent types. We quantified the dispersion in r_e/R_h for Illustris and IllustrisTNG, and investigated whether the residual in r_e/R_h (deviation from the median) correlates with halo spin. Lastly, we explored how individual galaxies evolve in r_e/R_h over their lifetimes.

Starting with the most basic point, it has been shown before that

Illustris predicts a very different relationship between galaxy mass and galaxy size than that predicted by IllustrisTNG – the galaxy sizes are about a factor of two larger in Illustris than in IllustrisTNG (Genel et al. 2014; Genel et al. 2018; Pillepich et al. 2018a). Clearly, this difference could reflect a difference either in the relationship (mean and/or dispersion) between stellar mass and halo mass, or in galaxy size and halo mass (size), or both. We have shown that the stellar mass vs. halo mass relation m_*/M_h is very similar for Illustris and IllustrisTNG at all redshifts from $z \sim 0$ to 2. This means that

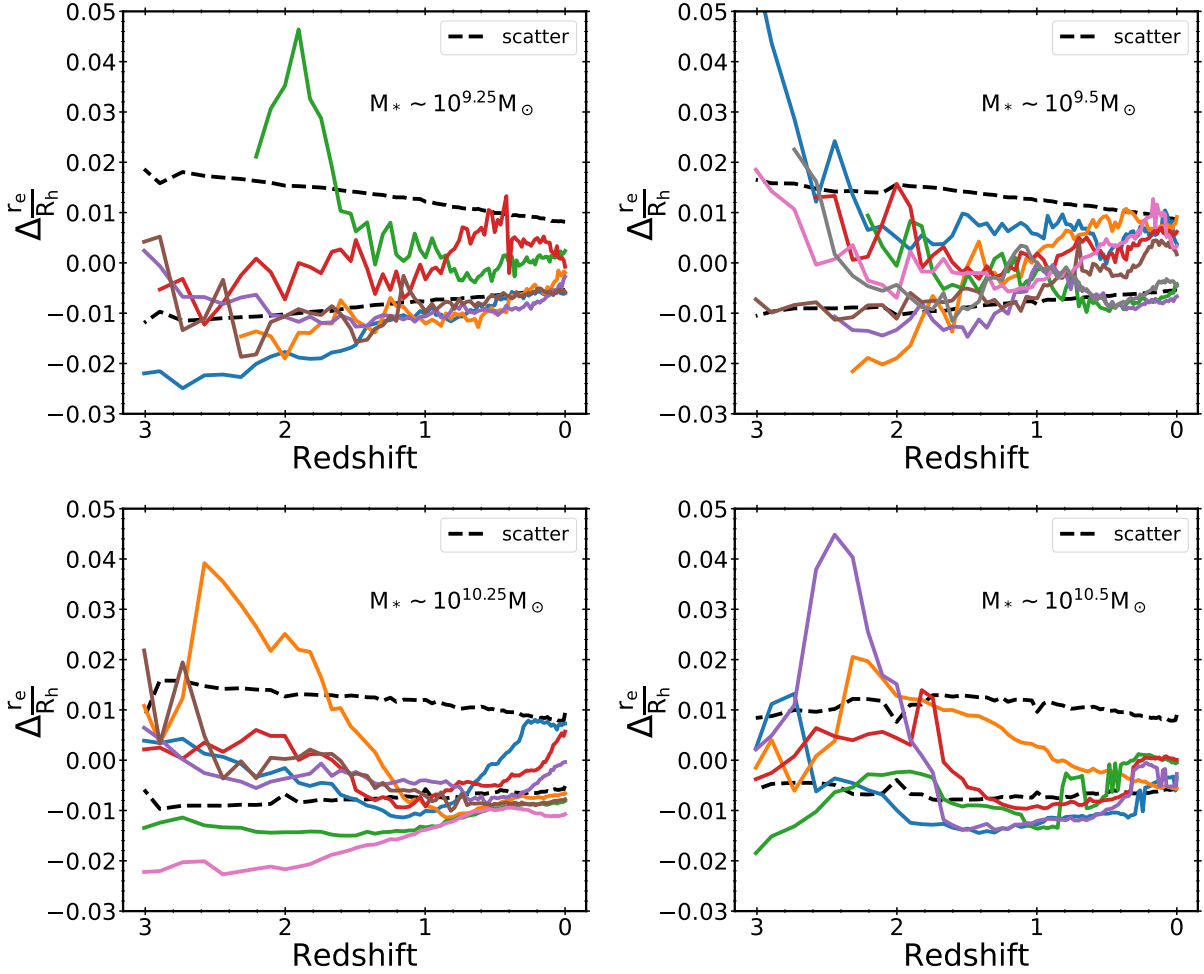


Figure 8. Redshift evolution of the residual (deviation from the median) of the stellar-to-halo size ratio r_e/R_h for sample galaxies with different stellar masses from IllustrisTNG. Dashed lines show the dispersion as calculated before. This illustrates that most galaxies oscillate around the median r_e/R_h relation during their evolution and suggests that the dispersion in the population at a given redshift arises from these oscillations.

the difference in the galaxy size-mass relation arises almost entirely from the difference in the size ratio r_e/R_h — somehow TNG haloes manage to assemble about the same mass of stars per unit total mass, but the stars are distributed very differently in radius. This is a bit surprising, as several studies have shown that varying the strength of stellar feedback often affects the slope and normalization of both m_*/M_h and r_e/R_h . For example, [Agertz & Kravtsov \(2016\)](#) showed the evolution over the lifetime of a fiducial Milky Way mass galaxy simulated with weak, fiducial, and strong feedback. They showed that weaker feedback resulted in a higher normalization and shallower slope for m_*/M_h , and a lower normalization and flatter slope for r_e/R_h . [Übler et al. \(2014\)](#) found similar results using a different code and feedback model.

When examining the behavior of r_e/R_h as a function of halo mass for the two simulations, it is apparent that not only is the normalization of r_e/R_h higher in Illustris than in IllustrisTNG at fixed M_h , but also that the dependence of r_e/R_h on M_h is much weaker in IllustrisTNG than in Illustris (Figure 2). Additionally, the difference between the normalization of r_e/R_h in IllustrisTNG and Illustris at fixed mass (halo or stellar) remains approximately constant

with redshift from $z \sim 3$ –0. These are all important clues to the physical processes that shape these relationships. Another important clue comes from examining both m_*/M_h and r_e/R_h for galaxies that have been divided into star-forming and quiescent populations (which could also be viewed as a rough proxy for disc-dominated and spheroid dominated galaxies). Surprisingly, both m_*/M_h and r_e/R_h are nearly the same for star-forming galaxies and quiescent galaxies in *both* Illustris and IllustrisTNG (with the exception of a slight upturn in r_e/R_h at the lowest halo masses, $M_h \lesssim 10^{10.5} M_\odot$, where this effect is stronger in Illustris). This is surprising from two angles: first, it is well known that in observations, quiescent galaxies have different stellar mass vs. size relations than star-forming galaxies, and these relations evolve differently with redshift for the two populations. It is not well established, however, to what extent this difference seen in populations reflects different overall evolutionary tracks in individual objects vs. “progenitor bias” ([van Dokkum et al. 2008](#); [Carollo et al. 2013](#); [Keating et al. 2015](#), and references therein). A related point is that using abundance matching, and assuming that all galaxies have the same SMHM relation, [Huang et al. \(2017\)](#) found that r_e/R_h was higher for galaxies in the highest quintile of sSFR than for those in

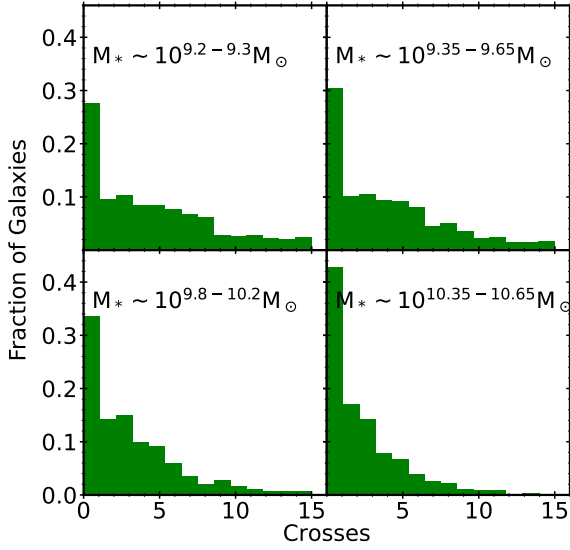


Figure 9. The number of times between $z = 3$ to $z = 0$ that IllustrisTNG galaxies cross the median stellar-to-halo size ratio as they evolve. The indicated mass limits correspond to the galaxy masses at $z = 0$. Most galaxies cross the median fewer than five times in their whole lifetime. However, between $\approx 60\% - 75\%$ of galaxies, depending on mass, do cross it at least once. With increasing stellar mass, the distribution becomes more skewed towards smaller values, with galaxies crossing the median less frequently.

the lowest quintile for the CANDELS sample. The second reason this result is surprising is that, from a theoretical point of view, one would expect star-forming and quiescent galaxies to evolve via different physical channels, where star-forming galaxies presumably grow mostly by accreting gas, while quiescent galaxies are thought to grow via gas poor mergers. One would expect these different channels to trace the evolution of dark matter haloes differently (we discuss this further in Section 5.3).

5.2 Physical origin of differences between Illustris and IllustrisTNG

The parameters for the IllustrisTNG simulations were tuned in light of several probes of galaxy properties, including the size-mass relation at $z = 0$ (Pillepich et al. 2018a). However, the physical origin of the different predicted size-mass relations in Illustris and IllustrisTNG is not well understood, although it is thought to be primarily connected to the sub-grid treatment of stellar driven winds. In both models, these winds are implemented by randomly selecting gas particles that are converted into “wind” particles, which are imparted a velocity “kick” and temporarily decoupled from hydrodynamic forces. The primary differences between the stellar wind implementation in IllustrisTNG relative to that in Illustris are (Pillepich et al. 2018a): 1) Velocity kicks are isotropic in direction rather than parallel to the rotation axis of the galaxy 2) The wind launch velocity has an additional redshift-dependent multiplicative factor, and a floor has been imposed 3) The wind mass loading factor (which in effect determines the overall probability that a gas particle will become a wind particle) has a dependence on the gas phase metallicity, such that the mass loading is higher for lower metallicity gas. The normalization is chosen such that the mass loading for L_* galaxies is similar in the two models,

implying that the mass loading for lower metallicity gas is higher in IllustrisTNG than in Illustris. In addition, IllustrisTNG includes magnetic fields, which were not included in the original Illustris simulations.

Figures 8, 10 and B1 of Pillepich et al. (2018a) show the effect of changing different pieces of the physics model in IllustrisTNG on both m_*/M_h and galaxy size vs. stellar mass. Switching off magnetic fields increases m_*/M_h by several tenths of dex for haloes more massive than a few times $10^{11} M_\odot$. The run with no magnetic fields leads to larger sizes at a fixed stellar mass by 20-30% at stellar masses less than $\sim 2 \times 10^{10} M_\odot$, and up to ~ 30 percent smaller sizes at higher stellar masses. Adopting non-isotropic winds, as in Illustris, leads to a very small change in galaxy size at fixed stellar mass relative to the TNG fiducial model. Dropping the metallicity-dependent mass loading scaling relation and removing the wind velocity floor has the largest effect on the size of any of the processes considered so far, increasing r_e by a factor of about 1.7 relative to the fiducial TNG model at a stellar mass $m_* \sim 10^{10} M_\odot$. None of the changes to the IllustrisTNG model, taken individually, account for the bulk of the change to the predicted sizes relative to the original Illustris simulation. Pillepich et al. (2018a) conclude that multiple processes (at least four) interact in a non-linear way to cause the difference in galaxy size predictions.

We note that both changes 2) and 3) above will make winds stronger and more effective at removing material at high redshift, and in low mass galaxies. Naively, one might have expected these changes to make galaxies *even* larger (as in general, “stronger” feedback leads to more extended discs; see above). One might also have expected a stronger redshift dependence to the emergent difference between r_e/R_h in the two models. The lesson seems to be that different implementations of stellar feedback lead to different qualitative effects on galaxy size and stellar mass, for reasons that are poorly understood. This is a topic that should be investigated systematically in the future.

5.3 Dispersion and its origin

Analytic and semi-analytic models of galaxy formation have commonly modeled disc sizes using the “angular momentum partition” ansatz (e.g. Mo et al. 1998; Dutton et al. 2007; Somerville et al. 2008; Porter et al. 2014; Henriques et al. 2015; Lacey et al. 2016). In this framework, it is assumed that the hot gas contained within a halo has the same spin λ as the halo, and that the gas that forms the disc has the same specific angular momentum j_d as the halo gas (or that it is related by a factor $f_j = j_d/j_h$, where j_h is the specific angular momentum of the halo gas). It is then expected that the disc effective radius is given by

$$r_e = \frac{1.68}{\sqrt{2}} f_j f_R(f_d, c_{\text{NFW}}, \lambda) \lambda R_h \quad (2)$$

where f_R is a function with a value of order unity that accounts for the effects of an NFW (Navarro et al. 1997) density profile, and for adiabatic contraction during the formation of the disc. This quantity is a weak function of the fraction of baryons in the disc (f_d), the NFW concentration c_{NFW} , and the spin parameter λ (see Somerville et al. 2008 for details). Based on this model, we would expect the dispersion in r_e/R_h to have a weak dependence on f_d and c_{NFW} , and a stronger dependence on λ . In this picture, the intrinsic dispersion in λ for dark matter haloes, which arises from their detailed collapse/merger histories, would give rise to most of the dispersion in galaxy size at fixed halo mass. Somerville et al. (2018) show that in this picture, the dispersion in λ found in dark matter only simulations is consistent with the observed dispersion in m_* vs. r_e .

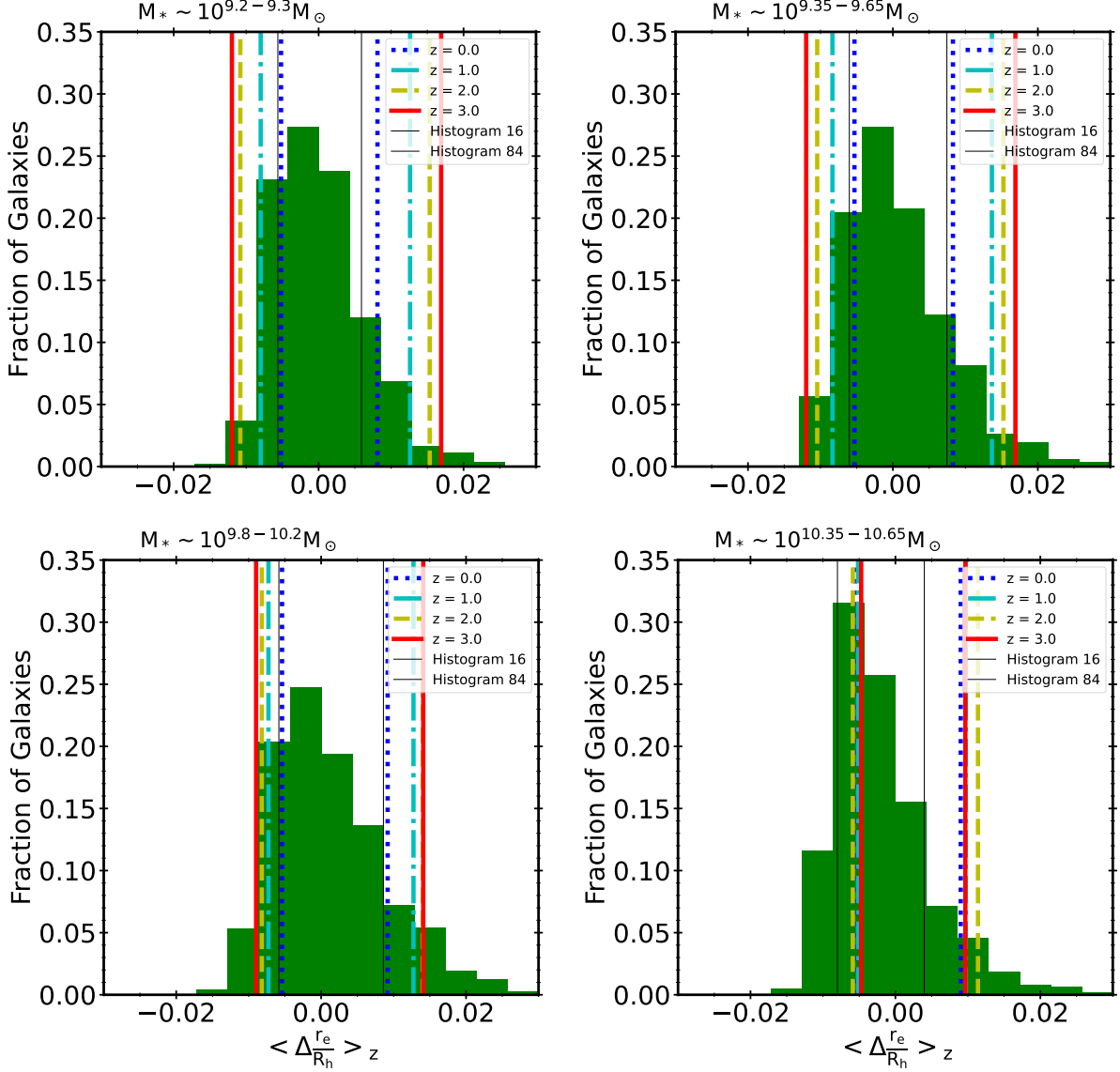


Figure 10. Histograms of the time-averaged residual of the stellar-to-halo size ratio of individual galaxies from the IllustrisTNG simulation between $z = 3$ to $z = 0$, with thin solid black lines representing the 16 and 84 percentiles of these histograms. The vertical lines (red, yellow, cyan, blue are for redshifts 3,2,1,0 respectively) represent the average 16 and 84 (left and right respectively) percentile spreads from Figure 6. The mass labels refer to the stellar masses at $z = 0$. The peak near zero with a width less than the average scatter values indicates that the scatter in Figure 6 is produced mostly due to galaxies oscillating around the median r_e/R_h relation, in agreement with Figure 9.

Several previous works have investigated the extent to which this model holds up for the galaxies produced in numerical hydrodynamic simulations. In general, these studies find no correlation or only a weak correlation between the residual in r_e/R_h and the halo spin parameter measured within the virial radius (Teklu et al. 2015; Zavala et al. 2016; Zjupa & Springel 2017; Desmond et al. 2017). Zanisi et al. (2020) showed that the scatter in the galaxy-halo size relation for late type galaxies could be interpreted due to the scatter in stellar angular momentum, instead of the halo spin parameter. Moreover, for late type galaxies at $z \sim 0$, Zanisi et al. (2020) found agreement between the dispersion in galaxy sizes in IllustrisTNG and semi-empirical constraints. Stronger correlations have sometimes been

found for sub-samples of specific types of galaxies in some simulations; for example, Yang et al. (2021) found stronger correlations between size and halo spin for Milky Way mass galaxies in the IllustrisTNG and AURIGA simulations that were selected via kinematics to be disc-dominated. However, they found weaker correlations for galaxies selected in the same way from the EAGLE and APOSTLE simulations. Jiang et al. (2019) also found a weak correlation between size and spin in the VELA and NIHAO zoom-in simulations, but did find a significant correlation between size and NFW halo concentration. In summary, the correlation between galaxy size and halo spin in hydrodynamic simulations seems to be dependent on the

galaxy selection criteria as well as the sub-grid physics implemented in the simulations.

For bulge-dominated galaxies, it is thought that galaxy size and mass growth are both predominantly driven by mergers. Gas-poor mergers tend to increase galaxy size, while gas-rich mergers decrease it (Covington et al. 2008; Naab et al. 2009; Hopkins et al. 2009; Covington et al. 2011; Oser et al. 2012). Thus the dispersion in galaxy size for these objects would be expected to correlate with the number of mergers experienced by a galaxy as well as the gas content of those mergers. Covington et al. (2008; 2011) and Porter et al. (2014) have presented results for the size evolution of bulge-dominated galaxies by implementing the size growth seen in binary merger simulations into a semi-analytic model, finding overall good agreement with observations (see also Shankar et al. 2013). To our knowledge, this has not been investigated in detail for large volume hydrodynamic simulations, but would be interesting to explore in the future.

6 CONCLUSIONS

We summarize our main findings and conclusions as follows:

- The relationship between stellar mass and halo mass is very similar in the Illustris and IllustrisTNG simulations from $z = 3-0$.
- Conversely, the relationship between galaxy radius and halo radius in Illustris and IllustrisTNG is very different. This implies that the very different galaxy stellar mass vs. size relationships in the two simulations are mainly due to the different predicted relationship between galaxy radius and halo radius.
- The r_e/R_h relation predicted by IllustrisTNG is in good agreement with constraints from structural abundance matching studies at low redshift. Illustris predicts a much stronger dependence of r_e/R_h on halo mass, with a normalization that is higher by about a factor of two. At high redshifts, IllustrisTNG too shows a stronger r_e/R_h dependence compared to the abundance matching results.
- Both Illustris and IllustrisTNG predict weak time evolution in r_e/R_h , in good agreement with the SHAM results of S18 and other similar studies.
- The relationships between stellar mass and halo mass, and galaxy size and halo size, are very similar for star-forming and quiescent galaxies in both Illustris and IllustrisTNG, at all redshifts from $z = 0-3$.
- We quantify the dispersion in r_e/R_h as a function of stellar mass, halo mass, and redshift, for both Illustris and IllustrisTNG. At $z \lesssim 1$, the dispersion is nearly constant with mass and has a value of around 0.01. At $z = 2$ and above, the dispersion decreases with increasing mass, and ranges from 0.005 to 0.02.
- There is only a weak correlation between the residual of r_e/R_h and halo spin, at all masses and redshifts that we investigated.
- When we track r_e/R_h over time for the main progenitor of a galaxy, we find that most galaxies oscillate around the median value of r_e/R_h several times during their lifetime, and that these oscillations are the dominant factor that gives rise to the dispersion in r_e/R_h .

In final conclusion, this work has continued the exploration of the link between galaxy structural properties and their haloes. We have demonstrated that quantifying the way in which galaxy properties relate to their host halo properties is a useful way to compare different simulations to one another, and also can provide useful insights into how simulations achieve or do not achieve agreement with observed scaling relations.

ACKNOWLEDGEMENTS

We would like to thank Ari Maller and the CCA galaxy formation group for valuable discussions. TK, RSS and SG acknowledge support from the Simons Foundation. TK also acknowledges support from the S.N. Bose Scholars Program, sponsored by the Science & Engineering Board (SERB), Department of Science and Technology (DST), Govt. of India, the Indo-U.S. Science and Technology Forum (IUSSTF) and WINStep Forward.

DATA AVAILABILITY

Illustris data is available for public access at <https://www.illustris-project.org/data/> and IllustrisTNG data can be found at <https://www.tng-project.org/data/>. S18 data and data analysis scripts are available upon request to the corresponding author.

REFERENCES

- Agertz O., Kravtsov A. V., 2016, *ApJ*, **824**, 79
 Behroozi P. S., Conroy C., Wechsler R. H., 2010, *ApJ*, **717**, 379
 Behroozi P., Wechsler R. H., Hearin A. P., Conroy C., 2019, *MNRAS*, **488**, 3143
 Blumenthal G., Faber S., Flores R., Primack J., 1986, *ApJ*, **301**, 27
 Brennan R., et al., 2015, *MNRAS*, **451**, 2933
 Brooks A., et al., 2011, *ApJ*, **728**, 51
 Bryan G. L., Norman M. L., 1998, *ApJ*, **495**, 80
 Carollo C. M., et al., 2013, *ApJ*, **773**, 112
 Covington M., Dekel A., Cox T. J., Jonsson P., Primack J. R., 2008, *MNRAS*, **384**, 94
 Covington M. D., Primack J. R., Porter L. A., Croton D. J., Somerville R. S., Dekel A., 2011, *MNRAS*, p. 1029
 Cui W., Davé R., Peacock J. A., Anglés-Alcázar D., Yang X., 2021, *Nat. Astron.*, **5**, 1069
 Dalcanton J., Spergel D., Summers F., 1997, *ApJ*, **482**, 659
 Desmond H., Mao Y.-Y., Wechsler R., Crain R., Schaye J., 2017, *MNRAS*, **471**, L11
 Dutton A. A., van den Bosch F. C., Dekel A., Courteau S., 2007, *ApJ*, **654**, 27
 Flores R., Primack J., Blumenthal G., Faber S., 1993, *ApJ*, **412**, 443
 Furlong M., et al., 2017, *MNRAS*, **465**, 722
 Genel S., et al., 2014, *MNRAS*, **445**, 175
 Genel S., et al., 2018, *MNRAS*, **474**, 3976
 Grogin N. A., et al., 2011, *ApJS*, **197**, 35
 Henriques B. M. B., White S. D. M., Thomas P. A., Angulo R., Guo Q., Lemson G., Springel V., Overzier R., 2015, *MNRAS*, **451**, 2663
 Hopkins P. F., Cox T. J., Younger J. D., Hernquist L., 2009, *ApJ*, **691**, 1168
 Huang K.-H., et al., 2017, *ApJ*, **838**, 6
 Jiang F., et al., 2019, *MNRAS*, **488**, 4801
 Keating S. K., Abraham R. G., Schiavon R., Graves G., Damjanov I., Yan R., Newman J., Simard L., 2015, *ApJ*, **798**, 26
 Koekemoer A. M., et al., 2011, *ApJS*, **197**, 36
 Kravtsov A. V., 2013, *ApJ*, **764**, L31
 Lacey C. G., et al., 2016, *MNRAS*, **462**, 3854
 Lange R., et al., 2015, *MNRAS*, **447**, 2603
 Liske J., et al., 2015, *MNRAS*, **452**, 2087
 Marinacci F., et al., 2018, *MNRAS*, **480**, 5113
 Mo H. J., Mao S., White S. D. M., 1998, *MNRAS*, **295**, 319
 Moster B. P., Somerville R. S., Maubetsch C., van den Bosch F. C., Macciò A. V., Naab T., Oser L., 2010, *ApJ*, **710**, 903
 Moster B. P., Naab T., White S. D. M., 2018, *MNRAS*, **477**, 1822
 Naab T., Ostriker J. P., 2017, *ARA&A*, **55**, 59
 Naab T., Johansson P. H., Ostriker J. P., 2009, *ApJ*, **699**, 178
 Naiman J. P., et al., 2018, *MNRAS*, **477**, 1206

- Navarro J. F., Steinmetz M., 2000, *ApJ*, 538, 477
- Navarro J. F., Frenk C. S., White S. D. M., 1997, *ApJ*, 490, 493
- Nelson D., et al., 2018, *MNRAS*, 475, 624
- Oser L., Naab T., Ostriker J. P., Johansson P. H., 2012, *ApJ*, 744, 63
- Peebles P. J. E., 1969, *ApJ*, 155, 393
- Pillepich A., et al., 2018a, *MNRAS*, 473, 4077
- Pillepich A., et al., 2018b, *MNRAS*, 475, 648
- Porter L. A., Somerville R. S., Primack J. R., Johansson P. H., 2014, *MNRAS*, 444, 942
- Rodríguez-Gomez V., et al., 2015, *MNRAS*, 449, 49
- Rodríguez-Puebla A., Behroozi P., Primack J., Klypin A., Lee C., Hellinger D., 2016, *MNRAS*, 462, 893
- Rodríguez-Puebla A., Primack J. R., Avila-Reese V., Faber S. M., 2017, *MNRAS*, 470, 651
- Shankar F., Marulli F., Bernardi M., Mei S., Meert A., Vikram V., 2013, *MNRAS*, 428, 109
- Shibuya T., Ouchi M., Harikane Y., 2015, *ApJS*, 219, 15
- Somerville R. S., Davé R., 2015, *ARA&A*, 53, 51
- Somerville R. S., et al., 2008, *ApJ*, 672, 776
- Somerville R. S., et al., 2018, *MNRAS*, 473, 2714
- Sommer-Larsen J., Gelato S., Vedel H., 1999, *ApJ*, 519, 501
- Springel V., White S. D. M., Tormen G., Kauffmann G., 2001, *MNRAS*, 328, 726
- Springel V., et al., 2018, *MNRAS*, 475, 676
- Steinmetz M., Navarro J. F., 2002, *New Astron.*, 7, 155
- Teklu A. F., Remus R.-S., Dolag K., Beck A. M., Burkert A., Schmidt A. S., Schulze F., Steinborn L. K., 2015, *ApJ*, 812, 29
- Übler H., Naab T., Oser L., Aumer M., Sales L. V., White S. D. M., 2014, *MNRAS*, 443, 2092
- Vogelsberger M., Genel S., Sijacki D., Torrey P., Springel V., Hernquist L., 2013, *MNRAS*, 436, 3031
- Vogelsberger M., et al., 2014a, *MNRAS*, 444, 1518
- Vogelsberger M., et al., 2014b, *Nature*, 509, 177
- Wechsler R. H., Tinker J. L., 2018, *ARA&A*, 56, 435
- Weinberger R., et al., 2017, *MNRAS*, 465, 3291
- Wuyts S., et al., 2012, *ApJ*, 753, 114
- Yang H., Gao L., Frenk C. S., Grand R. J. J., Guo Q., Liao S., Shao S., 2021, arXiv e-prints, p. [arXiv:2110.04434](https://arxiv.org/abs/2110.04434)
- Zanisi L., et al., 2020, *MNRAS*, 492, 1671
- Zavala J., et al., 2016, *MNRAS*, 460, 4466
- Zjupa J., Springel V., 2017, *MNRAS*, 466, 1625
- van Dokkum P. G., et al., 2008, *ApJ*, 677, L5
- van der Wel A., et al., 2014a, *ApJ*, 788, 28
- van der Wel A., et al., 2014b, *ApJ*, 788, 28

This paper has been typeset from a \LaTeX file prepared by the author.